Variability of the groundwater sulfate concentration in fractured rock slopes: a tool to identify active unstable areas

S. Binet[1,2,3,5], **L. Spadini**[2], **C. Bertrand**[3], **Y. Guglielmi**[4], **J. Mudry**[3], **and C. Scavia**[5]

[1]Institut des Sciences de la Terre d'Orléans – ISTO, UMR 6113, Université d'Orléans, CNRS/INSU, Université François Rabelais, Tours, Campus Géosciences, 1A, rue de la Férollerie, 45071 Orléans cedex 2, France
[2]Laboratoire de Géophysique interne et tectonophysique – LGIT, UMR 5559, Université Joseph Fourier, CNRS/INSU, Observatoire de Grenoble – BP 53, 38041 Grenoble, France
[3]Laboratoire de Chrono-Environnement – LCE, UMR 6249, Université de Franche-Comté, CNRS/INSU, France
[4]GéoSciences Azur (GA) – UMR6526, CNRS/INSU/IRD, UR082, Observatoire de la Cote d'Azur, Université de Nice Sophia-Antipolis, Université Pierre et Marie Curie, Paris VI, 250 rue A. Einstein, 06560, Valbonne, France

5415

[5] Dipartemento Ingegneria Strutturale e Geotecnica – DIST, Politecnico di Torino, Corso Duca Abruzzi 24, 10129 Torino, Italy

Correspondence to: S. Binet (stephane.binet@univ-orleans.fr)

Abstract

Water chemical analysis of 100 springs from the Orco and the Tinée valleys (Western Italy and Southern France) and a 7 years groundwater chemistry monitoring of the 5 main springs were performed. All these springs drain crystalline rock slopes. Some of these drain currently active gravitational slope deformations.

The pyrite nuclei contained in crystalline rock materials were found in the fractures to be covered superficially by iron oxide coatings. Potentially, the infiltration of oxidigenated waters leads to the dissolution of iron(II) sulfides associated with precipitation of insoluble iron(III) oxides and with a consequent release of sulfate ions to solution, such as observed.

All the waters flowing through unstable slopes show anomalies in the sulfate concentrations compared to stable aquifers. A sulfate concentrations increasing was observed repeatability after five consecutive landslides and suggest that the mechanical deformation is the origin of changes of the water composition and of the superficial mineralogy in the fractures. Moreover, the long-term observation of changes in water chemistry, rock mineral composition and associated calculation shows that sliding acceleration and chemical composition are closely related. Such signatures is produced even from slow (mm/yr) and low magnitude deformations. This result opens interesting perspective for the follow-up of sliding dynamic in landslides or in (a)seismic events and for the eventual prediction of catastrophic ruptures.

1 Introduction

The water in fractured rock is one of the major triggering factors that influence the rock stability (Keefer et al., 1987). The water saturation conditions determines the interstitial pressure. Changing the interstitial pressure may affect the stability of fractured rocks and cause fractures growth and landslide motions (Bonzanigo et al., 2001; Forlati et al., 2001). Such changes may induce a change in the infiltration conditions or a change

5417

in the groundwater pathways. These two parameters are thus linked to the interstitial pressure. Also, a primary slide may modify the pathways and the infiltration conditions that may affect durably the interstitial pressure and thus modify the overall stability of the rock masses.

~~The variability of cracks opening can be reasonably assumed that in these fractured areas the transfer times of individual water molecules differ strongly dependent on the chosen flow path.~~

The heterogeneity of the fractured rocks and their perpetual displacements makes it difficult to monitor their movements through installations of automated physical monitoring devices. Inside unstable masses such devices are readily broken and/or lost and need continuous survey. For these reasons, specific hydrogeochemical observation methods were developed (Vengeon, 1998; Guglielmi et al., 2000; Tullen, 2002) which focus on the monitoring of spring waters. The analysis of the water chemistry and flow rates allow to discuss the water/rock interactions (Guglielmi et al., 2000), the groundwater residence time (Bonzanigo et al., 2001) and the groundwater pathways (Mudry, 1990; Cappa et al., 2004) in chemically and mechanically active formations, for instance unstable slope.

The gravitational deformations induce a motion of the entire rocky slope, a propagation of discontinuities in the rock material (Barla and Chiriotti, 1996; Agliardi et al., 2001) and can generate additional cracks (Scavia, 1995), lead to a porosity and permeability changes (Binet et al., 2007c) and generate additional reactive surface areas, which in turn can change the chemical weathering rate and the groundwater chemistry.

The aim of the present study is to evidence the changing chemical signature of major ions flowing through gravitational active faults, and to correlate these signals to the motion of the rock masses in the given geological setting. The water chemistry in stable and unstable areas was intensively monitored. We show that the sulfate concentration can be used as a sensitive indicator of landslide movement. The changes in water chemistry, suggests that sliding velocity and chemical composition are closely related. Rock mineral composition within fractures and the associated modeling give a idea of

5418

the invoked mechanism. This result opens interesting perspectives for monitored the deformations and give a tool for an eventual prediction, of sliding or seismic events.

2 Material and methods

2.1 Study sites

"Tinée" (Southern Alps, France) and "Orco" (Rosone slope in the Eastern Alps, Italy) are two Alpine valleys composed of gneissic rocks (Fig. 1). These valleys are characterized by continuous landslide movements (Barla and Chiriotti, 1996; Casson et al., 2003), which forms the landscape from the post-glacial period (Julian and Anthony, 1996) . The past and actual landslides in these valleys may mobilize several millions of meter cubic of rock. Due to the inherent risk, both, Italian and French government authorities (Follacci, 1987; Amatruda et al., 2004) monitor the actually active slope deformations. The locations and velocities of actual movements are symbolized by grey surfaces of variable darkness (Fig. 1). Different kinds of deformation are observed. Toppling, in the higher part of the slopes (1500–2500 m a.s.l.), where cracks and trenches move typically some mm/yr (Fig. 1d). Downhills, the velocities of more than one meter per year were recorded 1997 and 2001, in the "La Clapière" landslide and about centimeters in 2001 in the "Rosone" landslide.

In the Tinée valley, groundwater infiltrates through fractured gneiss rocks at the top of the hillslope around 1500–2000 m a.s.l and moves consequently to the valley (1000 m a.s.l.) (Cappa et al., 2004; Binet et al., 2007b). Its flow through the cracks, until 100th meter under the ground surface, thereby increasing the pore pressure and thus participating to the landslide triggering (Cappa et al., 2004). Local high permeable Triassic deposits is pinched under the foot of the landslide (Feraud et al., 1975; Gunzburger and Laumonier, 2002).

In the Orco valley, water flows through a 10 m deep sub-surface aquifer (developed in the weathered gneisses and decompressed cracks of the slope. The groundwater

5419

recharge occurs locally in the upper part of the slope by infiltration at about 2500–1900 m a.s.l. The main outflow occurs downhill of the Rosone unstable area (around 1000 m a.s.l.) (Binet et al.,2007a).

2.2 Sampling and analysis of the Alpine crystalline rocks

A list of main minerals existing in the investigated areas is given in Table 1. The list was obtained from coupling own systematic observations from field trips (Binet et al., 2007a, 2007b) to previous works (Mazeran and Féraud, 1974; Féraud et al., 1975; Gunzburger and Laumonier, 2002).

During the field trips, the cracks, retained particular attention, especially when sliding patterns of rock were observed inside these fractures. The Fig. 4a presents an example of fractures (located by a cross in the Fig. 1c) dipping West in the slope direction reactivated by gravity deformation. The fractures, dipping East (i.e. perpendicular to the sliding direction), are non-reactivate (Guglielmi et al., 2005). Four Samples from these reactivated and non-reactivated cracks were carefully recovered to preserve the surface exposed to air and waters. 20 mm-sized particles were analysed with a Jeol 35 CF Scanning electronic microscope. Spot chemical analysis were obtained from a X-ray Fondis microprobe analyser.

2.3 Sampling and analysis of the Alpine crystalline basement ground waters

The water composition of a large number of the Tinée and the Orco valley springs was determined during the low water level periods. Each spring was classified dependent on the geological environment of catchment (draining gneiss rock, glacial or Triassic deposits) and on the stability of the corresponding formations (are some rock deformations known in the catchment or not?). The stability analysis was based on geomorphological observations, and on prior slope stability studies performed in these two valleys (Forlati et al., 2001; Julian and Anthony, 1996). The "La Clapière" region and the Rosone slope are known to be an very unstable area.

5420

In the Tinée valley, 92 springs were analyzed during an intensive campaign in august 2003 (Fig. 1c). On the Orco valley, 35 springs were analyzed in June 2004 (Fig. 1b).

In all these sites the waters evolved from soil to the Gneiss rock characteristics but in different environments of slope stabilities: unstable for S15 and S5 La Clapière (Tinée) and Bertodosca Rosone (Orco) springs, and stable for Luicetta (Tinée) and Moglia (Orco) springs. Corresponding sulfate and calcium data of those additional springs are given in Fig. 2 and Table 2 give the complete water chemical analysis for the main springs of the two valleys

Previous studies pointed that the S15 spring situated downstream of the landslide drains waters flowing through this unstable area (Guglielmi et al., 2000, 2002). The water composition and the temporal variability of the springs of this area were consequently studied in the frame of a seven year lasting long time survey (1998 and 2004). Table 3 presents the complete water chemical analysis of the S15 spring situated at the foot of the landslide for ten dates that characterize surrounding data, and the Fig. 3 represents the sulfate concentrations of the whole survey. During influenced stage (snow melting or rainfall), fresh waters dilute the springs water concentrations (circles in the Fig. 3) and brings nitrates from soil (Binet et al., 2007). The recession stages (Mudry, 1990) was defined when the nitrate concentration is null, with low dilutions of springs water concentrations (square in Fig. 3). Such exhaustive long-time surveys are not available for the other sites.

In all samples, dissolved K, Na, Ca and Mg concentrations were analyzed with a Perkin Elmer A Analyst 100 atomic absorption spectrometer (AAS), SO_4^{2-}, Cl^- and NO_3^- were obtained from High Pressure Ionic Chromatography (HPLC, Dionex DX 100), the HCO_3^- was obtained using strandard titrimetric methods. Detection limits are 0.005 and 0.002 mmol/L for AAS and HPLC tools, and the precisions are 5±1% for AAS, HPLC and alkalinity titration method.

5421

3 Results: field measurements of water quality and correlation with instabilities

3.1 Analysis of in situ gneiss matrix and fractures walls

Inside cracks, secondary minerals such as pyrite, calcite and amorphous Ferric oxides were found beneath the essential primary minerals forming the gneiss stone found everywhere else. The average composition of gneiss is about 66% of quartz, 3% of biotite, 8% of plagioclase (solid solution with 60% of anorthite and 40% of albite), and 4% of Kmica (Table 1) (Mazeran and Féraud, 1974; Féraud, 1975).

The microprobe analysis confirm the presence of S in active fractures, and the presence of Fe and O beneath the usual Si, Al, O, Na, Mg, K, Ca gneiss constituting elements composition. Image analysis revealed that the corresponding sulfur (Fig. 4b), and Fe oxide minerals (Fig. 4b), of active and inactive fractures are localized.

3.2 Characteristics of the water chemistry

The water chemical analysis were classified dependent on their geological environment and slope stability conditions. The waters (four samples) from soil have a 580–650 mV/H_2 redox values and the log of the CO_2 pressures, evolves from −0.6 to −0.9.

The waters from gneiss formations (quartz, biotite, Kmica, plagioclase and pyrite) are characterized by low Mg^{2+} concentrations, (0.02 to 0.18 mmol/L,) low electric conductivity (<500 µS/cm), and strongly variable SO_4^{2-} concentrations (0.03 to 0.79 mmol/L., Tables 2, 3 and Fig. 2).

Instead, the waters collected downstream Triassic formations are characterized by high SO_4^{2-} concentration (>1 mmol/L, "Mont Mounier" downhill springs and S15, Fig. 2a insert), high electrical conductivities (>500 µS/cm) and high Mg^{2+} concentration (>1.5 mmol/L). This suggests dissolution of Ca-Mg-SO_4 gypsum dolomite Triassic formations (Fig.1). This applied for example to the S15 spring (Table 3). This variability was already described in previous study (Guglielmi et al., 2000; Binet et al., 2007b). Such waters interacted supposedly with limestones, gypsum and pyrite.

5422

The Fig. 2 presents the SO_4 vs. Ca concentration ratios of the Tinée (Fig. 2a) and the Rosone slope (Fig. 2b) springs. The data are presented dependent on geological and geomorphological conditions, In both valleys, the water from gneiss rock type, are characterized by a constant SO_4/Ca ratio of 0.2–0.3. Triassic rock present a ratio of 1, but with an offset around 0.8 mmol/L of calcium for 0 mmol/L of sulfate. Waters flowing through Triassic rocks are thus characterised by 1 ratios with high concentration in calcium and sulfate. A ratio smaller than 0.05 ratio correspond to the glacial deposit types, which was only observed in the Rosone slope.

3.3 Sulfate concentrations in stable/unstable zones

In the Tinée valley the "La Clapière" (S15, S5, S6), "Noyere", "Pra" and "Saubieras" springs drain currently unstable areas (displacements of >1 mm/yr, gray shaded in the Fig. 1). In the Rosone slope three springs, 14, Bertodasco 5 and Perrebella 4, are known to be located in the moving zone (Fig. 1b, Amatruda et al., 2004). The SO_4/Ca concentration ratios of all these waters from unstable slope are higher or equal than 0.5 (big circles in Fig. 1), contrarily to all waters from stable zones (Fig. 2). This single parameter turns out to allow discrimination of moving versus non-moving zones. This means that the ground movements correlates with excess sulfate concentration in the waters compared to calcium.

The S15 spring is characterized by a particularly high SO_4 concentration during the recession stage. The long observation period of the S15 spring (Fig. 3) shows that the sulfate changes with time, and relates to the landslide acceleration (strong accelerations are grey shaded in Fig. 3). Thus in 1/1996 (1/1996 means first quarter of 1996), a high concentration (8.2 mmol/L) after an high acceleration is observed. It decreases then to 7.9 in the low movement period during until 4/1996. Similarly in 1999, after a relatively long low movement period (concentration at 6.2 in 2/1999), the concentrations increase to 7 in 4/1999. An short increase-decrease-increase of the concentrations from 6.8 to 8.8 to 6 to 6.5 mmol/L is also observed in 2000, and an overall decrease in 1/2002. Theses movements correlate qualitatively and positively to the landslide

acceleration.

4 Modeling of water rock interaction

4.1 Hydrochemical calculation with PHREEQC

Equilibrium calculations of rock-water systems were performed with the PHREEQC code and the integrated wateq4f database (Parkust and Appelo, 2004).

The modelled gneiss corresponds to the average composition of previously reported Tinée and Orco valley gneiss analysis (Féraud et al., 1975; Amatruda et al., 2004), except that biotite was replaced by phlogopite, i.e. the endmember of the phlogopite – siderophillite solid-solution system, as solubility data for the latter compound were not available.

The measured composition of soil water (analysis S in Table 2) contained 0.15 mmol/L of major ions, a pH value of 4.5 and a pCO_2 to $10^{-0.7}$ atm The low pH and high pCO_2 one side and the ionic composition on the other side represent respiration of infiltrating organic matter. The pH and pCO_2 values appear reasonable when compared to field observation data (Guglielmi et al., 2002). In these steep slopes, the soil is poorly developed. This soil water is considered infiltrating the deeper fractures and migrating downstream while undergoing chemical transformations. This water is considered representing the initial chemical composition of the flowing groundwater (Guglielmi et al., 2002). Once filtrated in the deeper fractures, the organic matter is considered entirely degraded and/or outfiltered and not further being supplied. This modeling hypothesis is supported from the oxygenated conditions found in all spring waters (Table 2, Eh data). CO_2 and O_2 are in excess in the script. This air open system will be discuss below.

In such a system, the gneiss dissolution becomes the dominant process. The pH will gradually increase when the primary minerals consume H^+ ions . The increasing pH leads finally to precipitation of insoluble mineral phases, and especially to precipitation

of $Al(OH)_3$ and $Fe(OH)_3$. It can be deduced from Table 1 that six, seven, or, respectively nine H^+ ions are consumed when dissolving one molecular unit of anorthite, albite, phlogopite or Kmica (in considering that Si is released as silicic acid $Si(OH)_4$, and Al as $Al(OH)_3$).

This basis hypothesis is inferred from the experimental data set, as all spring waters have higher pH and higher ion concentrations than the soil water. In concordance to field observations (Fig. 4), Fe-oxide and Al-oxide precipitation will occur. To note that the few OH^- ions bound to dissolved $Al(OH)_4^-$ and $Fe(OH)_4^-$ species are not significant compared to the the mass of dissolved OH^- ions.

The increase in pH will also lead to a decrease of the pCO_2 through transformation of disolved CO_2 into HCO_3^-. This and the concomitant release of Ca from the dissolution of primary minerals may lead to calcite precipitation. The Table 2 shows that 5 of the 13 reported springs have calcite saturation indices ≥ 0.5. In agreement with other studies (Guglielmi et al., 2000) this saturation indice is considered as the limit of calcite precipitation. The observed calcite in fractures and the other study about hydrochemistry of gneiss rock (Appello and Postma, 1996) indicate that calcite precipitation occurs in these systems and calcite was added as a equilibrium phase in the model

The presence of pyrite attested from field observations is considered to a source of Fe ions. The oxidation to sulfate and Fe^{+3}, with the associated precipitation of $Fe(OH)_3$ is a strongly proton-producing process (Eq. 1)

$$FeS_2 + 3.75\,O_2 + 3.5\,H_2O \Longleftrightarrow Fe(OH)_3 + 2\,SO_4^{2-} + 4\,H^+ \tag{1}$$
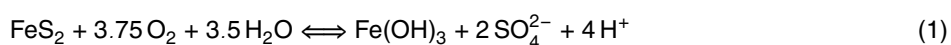
Finally, the presence of Gypsum is also attested in the Triassic deposits. Such deposits were observed in the Tinée valley close to the S15 springs and at the top of the Mounier mount (Fig. 1). No evidences were found around the Rosone slope, but as Gypsum is a highly soluble mineral, it was consequently included in all the models. This mineral increases $[SO_4^{2-}]$ and increases the saturation indices of calcite, i.e. promotes its precipitation. Concerning pH, the dissolution of the primary minerals increases pH, whereas precipitation of calcite (through deprotonation of HCO_3^- ions), Oxydation of

5425

pyrite and precipitation of iron oxides decreases the pH. Dissolution of Gypsum has no direct effect on pH.

The source and sink terms of individual ions can be outlined as follows: SO_4^{2-} is provided from pyrite and Gypsum. Silica, Al and OH^- are finally released from all primary minerals. On the side of precipitation calcite binds excess Ca and alkalinity, Fe precipitates as $Fe(OH)_3$, and Al precipitates as $Al(OH)_3$. As Silica gel and amorphous phases saturation index are negatives and as quartz phlogopite and Kmica have low kinetics of precipitation, these minerals can be over-saturated.

4.2 Inverse modeling

These processes and mineral phases were consequently implemented in the PhreeqC script. Soil water dissolves and/or precipitates a finite amount of each of the mineral phases listed in Table 1, the amounts are adjusted to fit the experimentally determined chemical composition of the spring waters. The proton balances are involved in these calculations. The calculations are applied to the 6 major springs (13 samples) draining gneiss fractures form the two study valleys (Table 2) and to the S15 spring (10 samples; approximately on per year) flowing through gneiss, with possible dolomite, gypsum and calcite presented in Table 3. The modeled amounts of gas and mineral dissolved needed to reproduce the spring water compositions are reported in Tables 2 and 3.

4.3 Dominent processes controlling the water quality

4.3.1 Origin of sulfates in silicate system waters deduced from Ph buffering processes

The Fig. 5a shows the evolution in pH and Ca^{2+} for variable amounts of dissolved gneiss (continuously increasing basis curve starting from the soil water), with or without contributions from dissolved pyrite and gypsum in calcite undersaturation conditions. Sulfate increase are induced from either a 0.1 mmol of pyrite, either a 0.2 mmol/L of

5426

gypsum dissolution, in a phlogopite+Kmica+plagioclase contents, respectively fixed to 0.2, 0.4, 0.6, 0.8 mmol/L. The dissolution of equivalent amounts of sulfate from pyrite or gypsum results in a decrease of pH (in case of pyrite) or in a increase of $[Ca^{2+}]$ (in case of Gypsum). These different effects allow to determine the origin of sulfate (pyrite versus gypsum) in the S5 spring. The inversed modelling suggest that S5(2), S5(3) and S5(6) dissolve 0.6 mmol/L of gneiss (Table 2). These data plotted in Fig. 5a shows that for fixed amount of dissolved gneiss the spring water pH decreases with time but not $[Ca^{2+}]$; more precisely between 0.1 and 0.8 mmol/L of pyrite needs to be dissolved, versus less than 0.1 mmol/L of Gypsum. The observed changes through time in sulfate concentration (S5(2), S5(3) and S5(6)) plotted in the Fig. 5 indicate that sulfate changes essentially originates from pyrite.

The interference between gypsum and pyrite in calcite saturated conditions are more complex (Fig. 5b). Dissolved Ca^{2+} will partly contribute to increase $[Ca^{2+}]$, and partly precipitate as calcite, decreasing by the way the alkalinity and the pH (through deprotonation of precipitating HCO_3^- ions). In Fig. 5b, Gypsum dissolution curves are thus no longer vertical. Concerning pyrite, the protons released (Eq. 1) will (as for Gypsum) displace the saturation pH of calcite to lower pH values, which means dissolution of calcite. In this case both, $[Ca^{2+}]$ and alkalinity increases, in difference to Gypsum dissolution. Parts of the protons contribute to lower the pH, and parts contribute to protonate the CO_3^{2-} ions released to solution from calcite. Thus, pyrite dissolution curves in Fig. 5b have also a negative slope. The S15 spring, saturated with respect to calcite, flows through gypsum and calcite. The sulfate content is very high (8 mmol/L) and may be explain by Gypsum located under the landslide (Gunzburger and Laumonier, 2002). The pH versus Ca plot of the S15 time series (Fig. 5b) shows that 2 to 5 mmol of Gypsum and 0 to 0.5 mmol/L of pyrite contributed to the sulfate measured in the spring. This shows that Gypsum dominantly contributed to the sulfate composition in this case, pyrite explain the recorded time evolution.

5427

4.3.2 O_2 and CO_2 conditions, and implications for open/closed model assumption

In the model, the introduced pyrite is entirely oxidized, as an excess oxygen concentration is introduced. This ensures that oxygenated conditions prevail at the spring outlet as experimentally determined (Tables 2 and 3). A priori this introduced "reactive pyrite" represents only a minor fraction of the FeS minerals existing in the field. Potentially much more pyrite may be really present, but associated to an insufficient contact time with water and/or surface area. The very low saturation indice of the pyrite (from −160 to −200) for a redox reaction confirm that pyrite is controlled by kinetics processes (Stefansson et al., 2005).

In the frame of the model assumptions the systems is considered at the equilibrium, however the spring water composition is controlled by a continuous dissolution process. The equilibrium model results represents a momentum analysis of kinetically driven reaction during transfer of water in the subsurface, which did not arrive at its end.

Following the pyrite oxidation Eq. (1), 3.75 oxygen atoms are needed to oxidise one sulphur atom to sulfate. O_2 saturated water at 5°C (Saturation $[O_2]aq$=0.4 mmol/L) may thus produce a maximum of 0.21 mmol/L sulfate from pyrite in a closed system. Most of the inversed O_2 values presented in the Table 2 and the Fig. 2 exceed this theoretical value by a factor of one or two. This means that the system is open for oxygen. Some surface oxygen supposedly diffuses into the groundwater, thus contributing to enhance the dissolved oxygen content needed for the oxidation of pyrite. Here, the groundwater flows mainly occur in the unsaturated zone in contact with gases (Binet et al., 2007b). Hydrogeological context is coherent with a opened system.

Note that the decrease of sulfate (Fig. 3) between 2002 and 2003 is regular that may discard a seasonal evolution of O_2 or CO_2 pressures or of the temperature that controlled the pyrite oxidation. In other areas, the dissolution of pyrite is insensitive to seasonal changes (Domenech et al., 2002).

pCO_2 values at the spring outlet (Tables 2 and 3) range between −3.32 and −2.7

5428

and are inferior to the atmospheric pCO_2 pressure ($pCO_2=10^{-3.5}$ atm). Even if the script is open to CO_2, the inversed model explains the pCO_2 decreasing only by a pH increase induced by gneiss dissociation. This further indicates that no CO_2 exchanges with the atmosphere occurred. More importantly, this shows that respiration processes, which would dramatically change the proton balance in the calculations, did not occur as such processes are known to disturb the groundwater pCO_2 values compared to the atmospheric pressure. This indicates that the soil organic matter was effectively outfiltered and/or entirely respirated in the early stage of the water flow in the soil, before flowing through the fractures. Deleted CO_2(g) in the script, to simulate a closed system do not modify the calculated solutions presented in Table 2. The soil alkalinity input is sufficient to explain the pCO_2 evolution with the pH increase.

4.4 Pyrite availability in unstable areas

The Tables 2 and 3 show the amounts of dissolved minerals used to explain the ground-water chemistry. Albite, anorthite and phlogopite explain more than 90% of the water chemistry acquisition (Table 2) and are considered as the main reactive minerals in gneiss. The sum of these 3 minerals is considered to represent the amount of dissolved gneiss. The chemistry of waters presented in Table 2 is explained with a dissolution from 0.08 to 3 mmol of gneissic rock and from 0.008 to 0.4 mmol of pyrite per liter. The waters from S15 dissolve from 1.9 to 2.9 mmol of gneiss, 2.9 to 5.5 mmol of Gypsum, 1.7 to 4 mmol of dolomite and 1.5 to 1.8 mmol of pyrite per liter.

The variability of these amounts is explained by hydrodynamic conditions that modify residence time of water (Mudry, 1990).

The dissolved amount of pyrite normed to the gneiss rock amount (Py/Gn) is an indicator of the relative pyrite weathering rate (Tables 2 and 3) the Py/Gn ratio range from 0.04 to 0.13 in stable aquifer and from 0.16 to 0.74 in unstable aquifers. The significant difference in the relative Py/Gn ratio suggests that the relative weathering rate of the pyrite is higher in the active fractures.

5429

5 Discussion

5.1 Relationship between physical erosion and chemical weathering

SO_4 time evolution could originate from a mix process, with waters from a pyrite rich reservoir. However the other ions in the water are not correlated with the accelerations. When the sulfate concentrations decrease, the Mg, Cl, Ca and HCO_3 concentrations can increase (see S15(7) and S15(8) in Table 3) or can decrease (see S15(0) and S15(1)). Thus mix process can be reasonably discard.

To discuss the origin of SO_4 time evolution requires taking into account an internal modification of dissolution rate of the pyrite correlated with landslide velocity. Within the fractures, the crystalline rock materials were found to be covered by iron oxide coatings (Fig. 4c) and inferred weathered fractures.

Sulfate anomalies were observed in all the water flowing trough active landslides in the two study valleys (Fig. 2). These sulfate increase were observed after 5 land-slide accelerations, and indicate that a mechanical deformation can (re) activate sulfate production. Thus, a mechanical effect can refresh the surfaces, reinitialize the disso-lution or create new fresh fractures (Fig. 4b). This mechanical effect can be linked to mechanical deformation of the slope, characterized in these valleys by complex pro-gressive failure propagation (Barla and Chiriotti, 1996).

During laboratory experiments of pyrite leaching, it appears that the dissolution rate decreases with time (Williamson and Rimstidt; 1994; Igarashi et al., 2003; Weisener et al., 2003). With time, the aging of mineral decreases the contact surface and the original behavior of pyrite dissolution cannot be re-established (Jerz and Rimstidt, 2004). Instance, with a 10 year observation scale, modifications of the groundwater chemistry in an acid moorland in the Welsh Uplands is attributed to a decrease in the weathering rate of pyrite (Forti et al., 1996). On the other side, at the continental scale, a theoretical model coupling chemical weathering and physical erosion in landslide-dominated landscapes is proposed to explain the refreshment of the weathering rate (Gabet, 2007). Here long term decrease of weathering rate and the theoretical refresh-

5430

ment are suggested at the landslide scale.

5.2 Implication for landslide management

A comparison of the weathering rates shows the possibility to localize current unstable areas with instantaneous measurements. This method enables to demonstrate the presence of a current unstable in the catchment. In these unstable mountainous contexts, the catchments of subsurface flows are localized. The waters infiltrates in the upper part of opened fractures and a part of this water outflow downhill from the bottom of these fractures (Binet et al. 2007). Performing sampling very close to the potential unstable area is possible to decipher if the sampled zone is moving or not.

If a potentially unstable slope is monitored, water chemistry is like a syn-deformation signal that can be use to recorded the fracture growing or the sliding evolution. With time, the fracture growing can lead to a catastrophic rupture (Scavia, 1995) and water chemistry can be a help to the prediction of this catastrophic rupture.

Stable area record a 0.13 to 0.4 Py/Gn ratio. In the moving area, Py/Gn ratio range between 0.16 to 0.74. Considering error range in the weathering rate values, a 0.15 value can be considered as a threshold value to discriminate stable and unstable area.

In the toppled area of the S5 spring, the 2 high ratios of the relative weathering rate of pyrite (0.4 for 1998 and 2000) suggest that the 2 last accelerations of the La Clapière landslide (1997 and 2000) have affected the entire hillslope. In this area, mm/yr displacements are estimated by stability calculations (Guglielmi et al., 2005). The hydrochemical signature is produced even from slow (mm/yr) and low magnitude (toppling) deformations.

The accelerations and the ruptures in the rock deformation have a very short time scale (form a second to a day).The changes in chemical signature of groundwater are related to transport of water (form a day to months in these subsurface context). However the rock deformations are often drived by cracks propagations or precursor slow movements (Scavia, 1995) that can be recorded by the water chemistry. In case where we can sample water close to (or in) a deformation area, the transport delay will

be reduced and the observed change in water chemistry may presents some prediction capacities.

6 Conclusions

Wet chemical analysis, from the Orco and the Tinée valleys (Western Italy and Southern France) were performed. Some of these springs drain currently active gravitational slope deformations. The groundwater sulfate concentrations increased from 0.1 to 1 mmol/L in the weeks following major displacement periods of a landslide.

The pyrite nuclei contained in gneissic rock materials were found in the fractures to be covered superficially by iron oxide coatings. Potentially, the infiltration of oxidigenated waters leads to the dissolution of iron(II) sulfides, associated precipitation of insoluble iron(III) oxides and consequent release of sulfate ions to solution. The sulfate anomalies concentration were observed in the 8 springs draining current active landslides compared to stable area. A sulfate concentrations increase was observed repeatability after five consecutive landslides evidencing that the mechanical deformation is at the origin of the changes of the water composition and of the superficial mineralogy in the fractures. Moreover, the long-term observation of changes in water chemistry, rock mineral composition and associated calculation suggests that sliding acceleration and chemical composition are closely related. The analysis of the sulfate concentrations appears to be a good proxy for the identification of gravitationally induced activities of a mountain rock slope.

This study show the possibility to constrain the localization of current unstable areas with instantaneous measurements of groundwater chemistry. The water chemistry is here like a syn-deformation signal that can be use to recorded the fracture growing, the sliding in a potentially unstable slope out of the deformation zone. Thus water quality brings clouds about the landslide dynamic outside of the landslide itself. Such signatures is produced even from slow (mm/yr) and low magnitude deformations. This result opens interesting perspective for the follow-up of sliding dynamic in landslides

or in (a)seismic events, for landslide event dating and for the eventual prediction of catastrophic ruptures if a fracture growing exists before the rupture.

References

Appelo, C. A. J. and Postma, D.: Geochemistry, groundwater and pollution, Book A. A. Balkema, Rotterdam, 1996.

Agliardi, F., Crosta, G., and Zanchi, A.: Structural constraints on deep-seated slope deformation kinematics, Eng. Geol., 59, 83–102, 1996.

Amatruda, G., Campus, S., Castelli, M., Piane, L., Forlatti, F., Morelli, M., Paro, L., Piana, F., Pirulli, M., Ramasco, M., and Scavia, C.:Identification And Mitigation Of Large Landslide Risks In Europe: Advances In Risk Assessment, edited by: Bonnard, C., Forlati, F., and Scavia, C., publisher: Balkema, A. A., Imiriland project, Torino, 2004.

Binet, S., Mudry, J., Scavia, C., Campus, S., Bertrand, C., and Guglielmi, Y.: In situ characterization of flows in a fractured unstable slope, Geomorphology, 86, 193–203, 2007a.

Binet, S., Guglielmi, Y., Bertrand, C., and Mudry, J.: Unstable rock slope hydrogeology: insights

5433

from the large-scale study of the western Argentera-Mercantour hillslopes (south-eastern France), B. Soc. Geol. Fr., 178, 159–168, 2007b.

Binet, S., Jomard, H., Lebourg, T., Guglielmi, Y., Tric, E. Bertrand, C., and Mudry, J.: Experimental analysis of groundwater flow through a landslide slip surface using natural and artificial water chemical tracers, Hydrol. Process., 21, 3463–3672, 2007c.

Barla, G. and Chiriotti, E.: Insights into the behaviour of the Large Deep Seat Gravitational Slope Deformation of Rosone, in the Piemont Region (Italy), Int. J. Rock Mech. Min., 33, 242–242, 1996.

Bonzanigo, L., Eberhart, E., and Loew, S.: Hydromechanical factors controlling the crfeeping Campo Vallemaggia, in: Symposium of landslides, causes, impacts and countermeasures, edited by UEF, Davos, 13–22, 2001.

Cappa, F., Guglielmi, Y., Soukatchoff, V. M., Mudry, J., Bertrand, C., and Charmoille, A.: Hydromechanical modeling of a large moving rock slope inferred from slope levelling coupled to spring long-term hydrochemical monitoring: example of the La Clapiere landslide (southern Alps, France), J. Hydrol., 291, 67–90, 2004.

Casson, B., Delacourt, C., Baratoux, D., and Allemand, P.: Seventeen years of the "La Clapiere" landslide evolution analysed from ortho-rectified aerial photographs, Eng. Geol., 68, 123–139, 2003.

Domenech, C., De Pablo, J., and Ayora, C.: Oxidative dissolution of pyritic sludge from the Aznalcollar mine (SW Spain). Chem. Geol., 190, 339–353, 2002.

Féraud, J., Picot, P., Pierrot R., and Vernet, J.: Métallogénie: sur la découverte de scheelite, cassitérite, bismuthinite et molydénite dans les gîtes à arsénopyrite du massif de l'Argentera. Conséquences métallogénétiques et pétrogénétiques, C. R. Acad. Sci. II, 280, 2179–2182, 1975.

Follacci, J. P.: Les mouvements du versant de la Clapière à Saint Etienne de Tinée (Alpes Maritimes), BLPC, 150, 107–109, 1987.

Forlati, F., Gioda G., and Scavia, C.: Finite element analysis of a deep-seated slope deformation, Rock Mech. Rock Eng., 34, 135–159, 2001.

Forti, M. C., Neal, C., and Robson, A. J.: Modelling the long-term changes in stream, soil and ground water chemistry for an acid moorland in the Welsh uplands: the influence of variations in chemical weathering. Sci. Total Environ., 180, 187–200, 1996.

Gabet, E. J.: A theoretical model coupling chemical weathering and physical erosion in landslide-dominated landscapes, Earth Planet Sci. Lett., 264, 259–265, 2007.

5434

Guglielmi, Y., Bertrand, C., Compagnon, F., Follacci, J. P., and Mudry, J.: Acquisition of water chemistry in a mobile fissured basement massif: its role in the hydrogeological knowledge of the La Clapiere landslide (Mercantour massif, southern Alps, France), J. Hydrol., 229, 138–148, 2000.

Guglielmi, Y., Vengeon, J., Bertrand, C., Mudry, J., Follacci, J., and Giraud, A.: Hydrogeochemistry: an investigation tool to evaluate infiltration into large moving rock masses (case study of the La Clapière and Séchilienne alpine landslides), Bull. Eng. Geol. Env., 61, 311–324, 2002.

Guglielmi, Y., Cappa, F., and Binet, S.: Coupling between hydrogeology and deformation of mountainous rock slopes: insights from La Clapiere area (southern Alps, France), C. R. Geosci., 337, 1154–1163, 2005.

Gunzburger, Y. and Laumonier, B.: A tectonic origin for the fold underlying the Clapiere landslide (NW Argentera-Mercantour massif, southern Alps, France) deduced from an analysis of fractures, C. R. Geosci., 334, 415–422, 2002.

Igarashi, T., Hataya, R., and Oyama, T.: Estimation of pyrite oxidation rate by sulfate ion discharged from a catchment, J. Geochem. Explor., 77, 151–165, 2003.

Jerz, J. K. and Rimstidt, J. D.: Pyrite oxidation in moist air, Geochim. Cosmochim. Ac., 68, 701–714, 2004.

Julian, M. and Anthony, E.: Aspects of landslide activity in the Mercantour Massif and the French Riviera, southeastern France, Geomorphology, 15, 275–289, 1996.

Keefer, D., Wilson, R. C., Mark, R. K., Brabb, E. E., Browm, W. M., Ellen, S. D., Harp, E. L., Wieczorek, G. F., Alger, C. S., and Zatkin, R. S.: Real-time landslide warning during heavy rainfall, Science, 13, 921–925, 1987.

Mazeran, R. and Féraud, J.: Sur la thermoluminescence des quartz filoniens à BPGC du massif de l'Argentera. Mise en évidence du caractère polyphasé de ces minéralisations, C. R. Acad. Sci. II, 278, 1147–1150, 1974.

Mudry, J.: Chemical mass flow vs. discharge and the functioning of karst aquifers, J. Hydrol., 120, 283–294, 1990.

Parkust, D. L. and Appelo, C. A. J.: PhreeQC2 user's manuel and programm, in: Water-Resources Investigations Report, edited by: US Geological Survey, 2004.

Scavia, C.: A method for the study of crack propagation in rock structures, Géotechnique, 45, 447–463, 1995.

Stefansson, A., Arnorsson, S., and Sveinbjornsdottir, A. E.: Redox reactions and potentials in

natural waters at disequilibrium, Chem. Geol., 221, 289–311, 2005.

Tullen, P.: Méthodes d'analyses du fonctionnement hydrogéologique des versant instables, Ph.D. thesis, ed. EPFL, Lausanne, 2002.

Vengeon, J. M.: Déformation et rupture des versants en terrain metamorphique anisotrope. Apport de l'étude des ruines de Séchilienne, Ph.D. thesis, edited by: University of Grenoble 1, Grenoble, 1998.

Weisener, C. G., Smart, R. S. T. C., and Gerson, A. R.: Kinetics and mechanisms of the leaching of low Fe sphalerite, Geochim. Cosmochim. Ac., 67, 823–830, 2003.

Williamson, M. A. and Rimstidt, J. D.: The kinetics and electrochemical rate-determining step of aqueous pyrite oxidation, Geochim. Cosmochim. Ac., 58, 5443–5454, 1994.

Table 1. Main and secondary minerals observed in the Orco and Tinée valleys. Molar percentage and chemical equations of the dissolution in a gneissic media are assessed for the La Clapière slope by (Guglielmi et al., 2000). logK values come from wateq4f database (Parkust and Appelo, 2004).

Minerals	% molar	log (K)	Dissociation equations
Quartz	66	−3.98	$SiO_2 + 2H_2O \Longleftrightarrow H_4SiO_4$
Kmica	4.1	11.63	$KAl_3Si_3O_{10}(OH)_2 + 9H_2O + H^+ \Longleftrightarrow K^+ + 3H_4SiO_4 + 3Al(OH)_3$
Phlogopite	3.0	−35.19	$KMg_3AlSi_3O_{10}(OH)_2 + 7H^+ + 3H_2O \Longleftrightarrow K^+ + 3Mg^{2+} + 3H_4SiO_4 + Al(OH)_3$
Plagioclase solid solution between:			
Albite	6.7	4.6	$NaAlSi_3O_8 + H^+ + 7H_2O \Longleftrightarrow Na^+ + 3H_4SiO_4 + Al(OH)_3$
Anorthite	1.3	−9.21	$CaAl_2Si_2O_8 + 2H^+ + 6H_2O \Longleftrightarrow Ca^{2+} + 2H_4SiO_4 + Al(OH)_3$
Secondary minerals			
Pyrite	–	−18.48	$FeS_2 + \frac{3}{4}O_2 + \frac{1}{3}H_2O \Longleftrightarrow 4H^+ + Fe(OH)_3 + 2SO_4^{2-}$
Fe oxides	–	4.89	$Fe(OH)_3 + 3H^+ \Longleftrightarrow Fe^{3+} + 3H_2O$
Gibbsite	–	8.11	$Al(OH)_3 + 3H^+ \Longleftrightarrow Al^{3+} + 3H_2O$
Gypsum	–	−4.58	$CaSO_4 \cdot 2H_2O \Longleftrightarrow Ca^{2+} + SO_4^{2-} + 2H_2O$
Halite	–	1.58	$NaCl \Longleftrightarrow Na^+ + Cl^-$
Dolomite	–	−16.54	$CaMg(CO_3)_2 \Longleftrightarrow Ca^{2+} + Mg^{2+} + 2CO_3^{2-}$
Calcite	–	−8.48	$CaCO_3 \Longleftrightarrow Ca^{2+} + CO_3^{2-}$

Table 2. Spatial variability of water quality recorded on the six major springs from the two studies valleys. S5 refers to the spring of the La Clapi'ere (Tinée) site. Calculated values of the saturation index and inversed values of the range of percentage of dissolved minerals.

Spring		S5						Luicetta		Gallery		Bertod.	Moglia	Gera	Soil
Sample ID		S5(1)	S5(2)	S5(3)	S5(4)	S5(5)	S5(6)	L(1)	L(2)	G(1)	G(2)	B(1)	M(1)	Ge(1)	S
Sampling date		12/98	04/99	09/00	06/02	08/03	04/04	05/03	07/04	03/03	04/04	06/04	06/04	06/04	03/03
Aquifer type		Toppling zone						Stable		Stable		Unstable	Stable	Stable	Soil
Location		Tinee valley						Tinee valley		Tinee valley			Rosone		
Measured values															
Velocity	(mm/mo)	< 1	< 1	< 1	< 1	< 1	< 1	/	/	/	/	10	/	/	/
Rain	(mm/mo)	34	117	97	57	40	72	0	0	0	72	0	0	0	
Yield	(l/s)	/	0,10	0,10	0,10	0,1	0,15	4,75	4,5	0,05	0,01	2,0	5	0,7	/
Conductivity	(µS/cm)	199	136	229	160	189	158	152	162,6	400	333	28	60	84	28
Temp	(°C)	8,2	8,0	12,0	10,0	11,3	7,7	9,9	11,9	10,1	11,3	6,1	8,1	7	6,40
pH		7,5	7,1	7,9	8,0	7,5	6,9	8,1	8,0	7,9	8,2	7,7	8,0	8,2	4,50
Eh	mV/H2				460		455		460						625
HCO_3^-	(mmol/L)	1,20	0,90	0,80	0,80	0,84	0,72	1,1	1,08	2,55	2,29	0,20	0,42	0,44	0,10
Cl^-	(mmol/L)	0,02	0,02	0,06	0,02	0,08	0,03	0,03	0,04	0,05	0,06	0,02	0,02	0,15	0,02
SO_4^{2-}	(mmol/L)	0,48	0,28	0,53	0,50	0,51	0,38	0,19	0,17	0,79	0,59	0,05	0,06	0,07	0,03
Ca^{2+}	(mmol/L)	0,70	0,51	0,56	0,70	0,78	0,47	0,65	0,62	1,85	1,50	0,06	0,18	0,21	0,03
Mg^{2+}	(mmol/L)	0,18	0,12	0,19	0,12	0,13	0,17	0,09	0,09	0,12	0,12	0,02	0,03	0,05	0,02
Na^+	(mmol/L)	0,38	0,21	0,22	0,20	0,29	0,26	0,15	0,11	0,22	0,2	0,07	0,08	0,23	0,02
K^+	(mmol/L)	0,04	0,04	0,07	0,04	0,04	0,06	0,02	0,03	0,03	0,03	0,04	0,05	0,03	0,02
NO_3^-	(mmol/L)	0,006	0,019	0,016	0,006	0,006	0,024	0,006	0,006	0,006	0,015	0,035	0,031	0,019	0,000
SO_4 / Ca		0,69	0,55	0,94	0,71	0,66	0,81	0,29	0,28	0,43	0,39	0,76	0,33	0,32	0,83
Electrical balance %		0,2	-0,8	3,4	-1,6	-4,9	-2,5	-4,6	-3,3	0,0	0,6	3,3	0,8	-5,1	8,57
Calculated values															
Fe	(mmol/L)	3E-06	4E-06	4E-06	3E-06	3E-06	3E-06	2,7E-06	4E-06	3E-06	3E-06	1E-06	2E-06	2E-06	4E-4
P_{CO2}	log(atm)	-2,7	-2,4	-3,2	-3,4	-2,8	-2,3	-3,3	-3,3	-2,8	-3,2	-3,5	-3,3	-3,5	-0,70
Eh	mV/H2	551	597	460	460	462	457	417	482	542	417	435	478	441	630
SI pyrite		-181	-190	-172	-169	-191	-198	-164	-192	-179	-177	-192	-176	-172	-220
SI gypsum		-2,1	-2,5	-2,2	-2,1	-2,1	-2,4	-2,5	-2,6	-1,6	-1,8	-4,0	-3,5	-3,4	-4,39
SI calcite		-0,9	-1,5	-0,7	-0,5	-0,9	-1,8	-0,3	-0,4	0,3	0,5	-1,9	-1,6	-1,2	-5,60
Inversed values															
Pyrite	mmol/L	0,22	0,13	0,25	0,24	0,24	0,18	0,08	0,08	0,38	0,29	0,01	0,01	0,02	
Albite	mmol/L	0,36	0,19	0,16	0,18	0,21	0,23	0,12	0,11	0,17	0,14	0,06	0,06	0,08	
Anorthite	mmol/L	0,56	0,45	0,59	0,65	0,73	0,46	0,53	0,51	2,84	2,84	0,01	0,13	0,36	
Phlogopite	mmol/L	0,04	0,02	0,06	0,03	0,03	0,04	0,02	0,02	0,03	0,03	0,01	0,01	0,01	
Calcite	mmol/L	/	/	/	/	/	/	/	/	-1,03	-1,36	/	/	/	
Gibbsite	mmol/L	-1,53	-1,11	-1,40	-1,52	-1,7	-1,2	-1,21	-1,17	-5,88	-5,86	-0,12	-0,33	-0,8	
$Fe(OH)_3(a)$	mmol/L	-0,22	-0,12	-0,25	-0,23	-0,24	-0,17	-0,08	-0,08	-0,38	-0,29	-0,01	-0,02	-0,02	
$O_2(g)$	mmol/L	0,84	0,47	0,94	0,88	0,92	0,65	0,31	0,3	1,43	1,07	0,03	0,06	0,08	
$CO_2(g)$	mmol/L	0	0	0	0	0	0	0	0	0	0	0	0	0	
Gneiss=Σal.+An.+Phlo.		0,96	0,66	0,81	0,86	0,97	0,73	0,67	0,65	3,03	3,02	0,08	0,2	0,45	
Py/ Gneiss	mmol/L	0,23	0,2	0,31	0,28	0,25	0,25	0,12	0,12	0,13	0,1	0,16	0,05	0,04	

(Input data for calculation)

Table 3. Temporal variability of water quality recorded on the S15 springs draining the La Clapière landslide. Calculated values of the saturation index and inversed values of the range of percentage of dissolved minerals (Yields values presented in italic are estimated).

Spring		S15									
Sample ID		S15(0)	S15(1)	S15(2)	S15(3)	S15(4)	S15(5)	S15(6)	S15(7)	S15(8)	S15(9)
Sampling date		04/96	12/98	05/99	07/00	02/01	04/01	11/01	06/02	09/03	04/04
Aquifer type		Moving zone: La Clapière landslide									
Measured values											
Velocity	(mm/mo)	1500	36	23	66	1437	1241	35	8	22	21
Rain	(mm/mo)	/	34	90	158	106	31	24	57	71	72
Yield	(l/s)	0,20	0,15	0,10	*0,10*	*0,10*	*0,10*	*0,10*	*0,10*	*0,10*	0,12
Conductivity	(µS/cm)	1496	1440	1404	1331	1518	902	1523	1508	1519	1198
Temp	(°C)	11,3	8,2	16,6	20,0	9,7	9,4	9,6	12,1	12,4	9,7
pH		7,2	8,0	7,9	7,4	8,1	7,5	*8,0*	7,7	7,9	8,2
Eh	mV/H2								515		453
HCO_3^-	(mmol/L)	2,88	3,64	3,00	1,50	1,72	1,25	3,68	3,72	3,68	2,00
Cl^-	(mmol/L)	0,09	0,17	0,15	0,13	0,13	0,20	0,12	0,18	0,10	0,13
SO_4^{2-}	(mmol/L)	8,55	6,76	6,24	6,33	7,45	6,34	7,33	7,92	6,27	6,11
Ca^{2+}	(mmol/L)	4,50	5,75	5,95	4,65	6,12	4,42	5,85	6,35	4,50	4,50
Mg^{2+}	(mmol/L)	4,46	2,23	1,98	2,14	2,29	1,98	2,35	2,52	3,22	1,95
Na^+	(mmol/L)	0,72	0,99	0,70	0,86	0,81	0,71	0,84	0,84	0,74	0,94
K^+	(mmol/L)	0,15	0,15	0,15	0,19	0,22	0,19	0,22	0,19	0,12	0,23
NO_3^-	(mmol/L)	0,000	0,000	0,000	0,000	0,000	0,003	0,000	0,013	0,011	0,005
SO_4 / Ca		1,9	1,2	1,1	1,4	1,2	1,4	1,3	1,3	1,4	1,4
Electrical balance %		3,3	0,7	-3,3	-1,2	-3,2	1,8	2,8	2,6	0,0	1,0
Calculated values											
Fe	(mmol/L)	2E-6	2E-06	8E-06	2E-05	3E-06	4E-06	3E-06	4E-06	4E-06	3E-06
P_{CO2}	log(atm)	-3,36	-2,75	-2,58	-2,51	-3,22	-2,91	-3,13	-2,50	-3,35	-3,29
Eh	mV/H2	550	457	552	562	542	566	479	513	525	412
SI pyrite		-181	-184	-192	-185	-168	-188	-176	-179	-179	-161
SI gypsum		-0,50	-0,49	-0,59	-0,61	-0,49	-0,64	-0,52	-0,48	-0,84	-0,65
SI calcite		0,30	0,77	0,82	-0,10	0,57	-0,55	0,44	0,58	-1,45	0,55
SI albite		-4,60	-4,09	-4,07	-4,37	-4,03	-4,69	-4,02	-4,33	-4,18	-3,76
Inversed values											
Pyrite	mmol/L	1,57	0,66	1,28	1,27	1,23	1,77	1,80	1,7	1,53	1,50
Gypsum	mmol/L	4,27	5,73	3,97	3,93	5,33	2,93	3,33	4,03	3,17	2,95
Plagioclase An60	mmol/L	2,10	2,69	1,83	2,43	2,27	1,7	2,4	2,2	2,13	2,7
Phlogopite	mmol/L	0,13	0,13	0,13	0,17	0,2	0,68	0,2	0,17	0,1	0,21
Dolomite	mmol/L	4,00	1,7	1,57	1,62	1,67	1,96	1,73	1,99	2,91	1,31
Calcite	mmol/L	-0,9	-2,96	-1,15	-2,66	-2,69	0,26	-0,81	-1,16	-3,13	-1,7
Gibbsite	mmol/L	-3,72	-4,69	-3,25	-4,31	-4,05	-3,57	-4,28	-3,91	-3,73	-4,8
$Fe(OH)_3(a)$	mmol/L	-1,51	-1,83	-1,28	-1,27	-1,23	-1,77	-1,8	-1,73	-1,53	-1,49
$O_2(g)$	mmol/L	5,62	2,49	4,78	4,77	4,62	6,63	6,75	6,5	5,74	5,62
$CO_2(g)$	mmol/L	0	0	0	0	0	0	0	0	0	0
Gneiss=ΣPla.+Phlo.	mmol/L	2,13	2,82	1,96	2,6	2,47	2,39	2,6	2,37	2,23	2,91
Py / Gneiss	mmol/L	0,74	0,23	0,65	0,49	0,5	0,74	0,69	0,72	0,69	0,52

5439
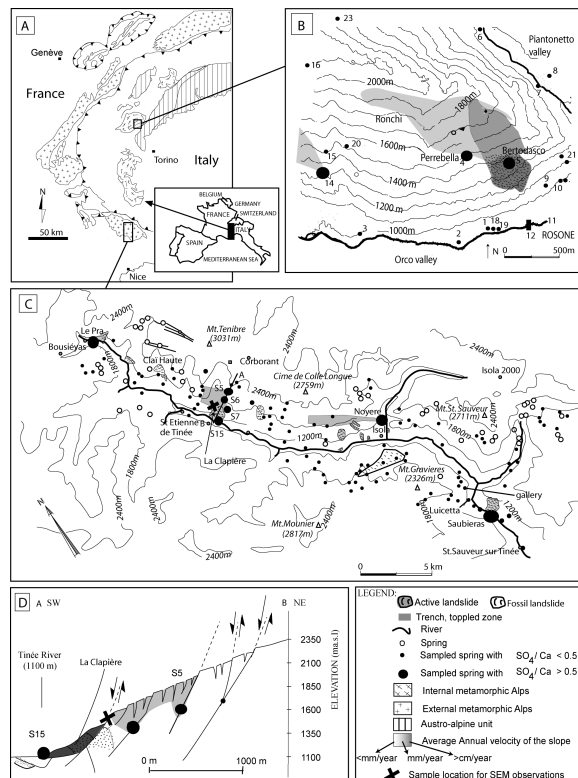
Fig. 1. Structural map of the Alps with detailed map of **(A)** the Rosone slope (Grande Paradiso) and **(B)** the Tinée Valley (Mercantour massif). **(C)** Schematic geological cross section through the "La Clapière" landslide, and localization of the monitored springs.

5440
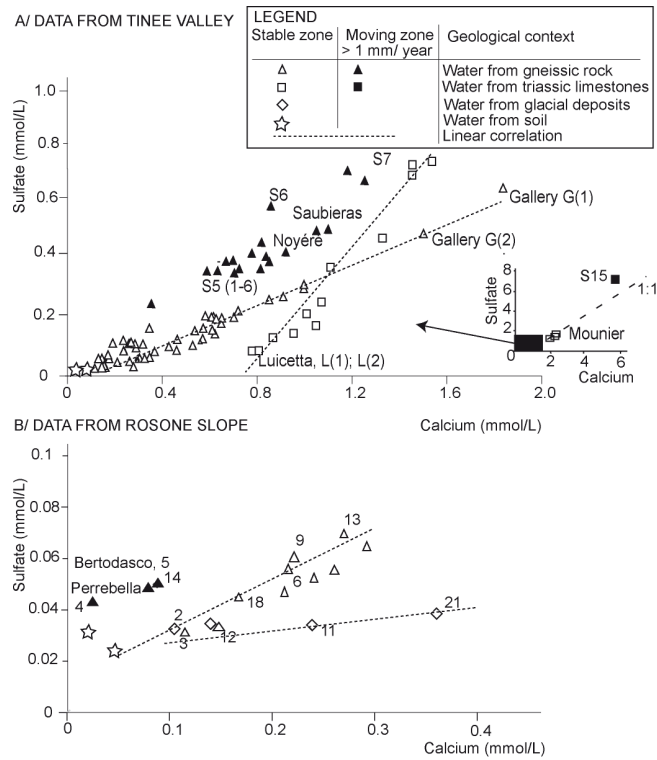
Fig. 2. Spatial variability of solute concentration measured in the springs of gneissic aquifers: **(A)** in the Tinée valley (S15 is in an insert) and **(B)** in the Rosone slope. The symbol form is related to the geological context, the back symbol are related to spring draining a unstable slope.
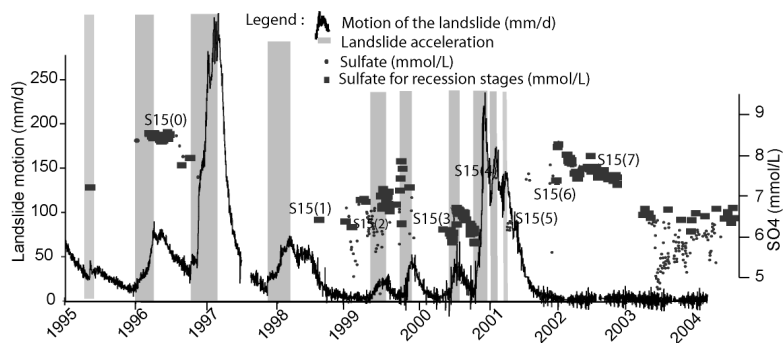
Fig. 3. Temporal evolution of the sulfate concentration measured in a spring draining an active unstable area (La Clapière landslide). The circles present the whole measurements, the squares, the measurments realized when nitrate concentration is null (recession stage). The sulfates changes during recession stage are related with the landslide velocity (strong accelerations are grey shaded). Sulfate concentration of year 1998 are not exploitable. The S15(1, 2, ...) annotations, refer to complete analysis of the S15 trough time, presented in the Table 3.
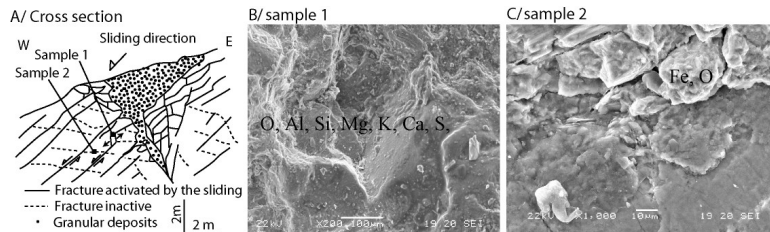
Fig. 4. Localization and observations of fracture walls: **(A)** Localization of fractures in cross-section with sliding displacements along fracture dipping towards West **(B)** electronic micro-scope and micro-probe results in an active (dipping west, sample 1) fractures and **(C)** in an inactive (dipping Est, sample 2) fracture covered with a thin ferric layer.
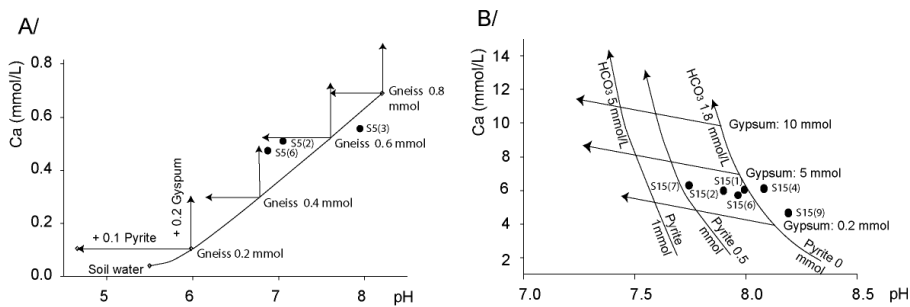
Fig. 5. Calculated evolution of pH and calcium content related to a 0.2 mmol/L sulfate increase in water flowing in gneiss rock and comparison with field measurments. **(A)** Evolution in pH and Ca^{2+} for dissolving gneiss (continuously increasing basis curve starting from the soil water), with or without contributions from pyrite and gypsum in calcite undersaturation conditions. Sulfate increase are induced from either a 0.1 mmol of pyrite, either a 0.2 mmol/L of gypsum dissolution, in a phlogopite+Kmica+plagioclase contents fixed to 0.2, 0.4, 0.6, 0.8 mmol/L, in an under-saturated water in respect to calcite. Model is confronted to S5 springs measurements dissolving approximately 0.6 mmol/L of gneiss, presented in Table 2. **(B)** Sulfate increase are induced from either a 0.1 mmol of pyrite dissolution in gneiss, either a 2 mmol/L of gypsum dissolution in gneiss buffered context (fixed alkalinity=1 mmol/L, phlogopite+K-mica+plagioclase content=0.2 mmol/L) in an oversaturated water in respect to calcite. Model is confronted to S15 springs measurements presented in Table 3.